



# Tendency in tip polarity changes in non-contact atomic force microscopy imaging on a fluorite surface

Bob Kyeyune, Philipp Rahe and Michael Reichling\*

## Full Research Paper

Open Access

Address:

Institut für Physik, Universität Osnabrück, Barbarastrasse 7, 49076 Osnabrück, Germany

*Beilstein J. Nanotechnol.* **2025**, *16*, 944–950.

<https://doi.org/10.3762/bjnano.16.72>

Email:

Michael Reichling\* - [reichling@uos.de](mailto:reichling@uos.de)

Received: 13 March 2025

Accepted: 03 June 2025

Published: 26 June 2025

\* Corresponding author

This article is part of the thematic issue "At the cutting edge of atomic force microscopy".

Keywords:

atomic resolution imaging; calcium fluoride surface; interaction force; non-contact atomic force microscopy (NC-AFM); tip change

Associate Editor: T. Glatzel



© 2025 Kyeyune et al.; licensee Beilstein-Institut. License and terms: see end of document.

## Abstract

We investigate the impact of tip changes on atomic-scale non-contact atomic force microscopy (NC-AFM) contrast formation when imaging a  $\text{CaF}_2(111)$  surface. A change of the atomic contrast is explained by a polarity change of the tip-terminating cluster or by a polarity-preserving tip change via the re-arrangement of the foremost atoms. Based on the established understanding of the unique contrast patterns on  $\text{CaF}_2(111)$ , polarity-preserving and polarity-changing tip changes can be identified unambiguously. From analyzing a large set of images, we find that the vast majority of tip changes tend to result in negative tip termination. This analysis delivers hints for tip configurations suitable for stable imaging of  $\text{CaF}_2(111)$  surfaces.

## Introduction

Non-contact atomic force microscopy (NC-AFM) [1] is a surface science tool that has been used to atomically resolve surfaces of semiconductor and insulator materials in real space with unprecedented spatial resolution [2-6]. Besides high-resolution imaging of molecular structures [7], NC-AFM has demonstrated its ability to identify sublattices of atomic surfaces [8-10]. In these studies, the knowledge of the tip's atomic structure plays a vital role as the tip-terminating cluster uniquely interacts with the different surface atoms. At cryogenic temperatures, the use of functionalized tips such as as

CO-terminated tips [6,11], Xe-terminated tips [12-14] and O-terminated Cu tips [15-17] has become the state-of-the-art for structure elucidation and identification of surface sites.

However, this approach is presently not feasible for measurements performed at room temperature as the required control over the tip termination is challenged by thermal motion. For room-temperature measurements, it is common practice to bring the tip apex in slight contact with the surface under investigation to form a tip cluster yielding atomic contrast [18]. As struc-

ture and chemical composition of the resulting tip-terminating cluster are not known, the understanding of contrast formation with non-functionalized tips has been developed over many years based on theoretical simulations of NC-AFM data for a variety of plausible tip models [9,19–22]. Through further endeavors, a qualitative distance-dependent approach involving electrostatic interactions and Pauli repulsion has recently been exemplified on  $\text{CaF}_2(111)$  [10]. As a central result, gradual atomic contrast transitions as a function of the tip–sample distance have been introduced as criteria for identifying a positively and a negatively terminated tip [10]. Still, a crucial aspect in sublattice identification studies is to distinguish between contrast changes caused by a change of the tip-terminating cluster (i.e., a tip change) and a distance-dependent contrast evolution for a stable tip. Tip changes are inevitable in NC-AFM experiments with non-functionalized tips, especially as commonly used silicon tips are very reactive and readily pick up various entities. This particularly concerns the transfer of surface species to the tip when the tip is subject to intentional or unintentional contact with the surface. Furthermore, ambient species like native oxides, hydrogen ions, or residual water can adsorb on the tip apex during scanning. Additionally, the foremost tip atom may rearrange to minimize the tip surface energy in response to increasing tip–sample interaction forces.

Here, we perform an experimental investigation of tip changes during NC-AFM imaging of a  $\text{CaF}_2(111)$  surface with non-functionalized tips at both room temperature (RT) and low temperature (LT). We identify atomic contrast changes resulting either from a polarity change of the tip-terminating cluster or from a polarity-preserving tip change. Following the recently developed model for contrast formation on  $\text{CaF}_2(111)$  surfaces [10], we adopt the contrast mode notations  $\mathbf{C}_1$ ,  $\mathbf{C}_3$ , and  $\mathbf{C}_4^*$  for a positively terminated tip and  $\mathbf{C}_2$  and  $\mathbf{C}_4$  for a negatively terminated tip. The distance-dependent contrast evolution [10] is summarized along the vertical columns in Figure 1. This figure additionally includes markers for tip changes as demonstrated in this work: Black solid arrows mark contrast changes exhibiting a change in tip polarity demonstrated in this work, while polarity-preserving tip changes are indicated by grey arrows. In addition, dashed arrows denote polarity changing tip changes that were observed during our experiments but are not discussed in the following as they represent the reverse direction of presented cases.

The contrast modes  $\mathbf{C}_4$  or  $\mathbf{C}_4^*$  are cyclic members of the same contrast mode, as introduced in [10]. Consequently, the assignment of NC-AFM image data to these contrasts modes requires the acquisition of systematic distance-dependent measurements [10]. Without such distance-dependent data, the contrast mode assignment is questionable.

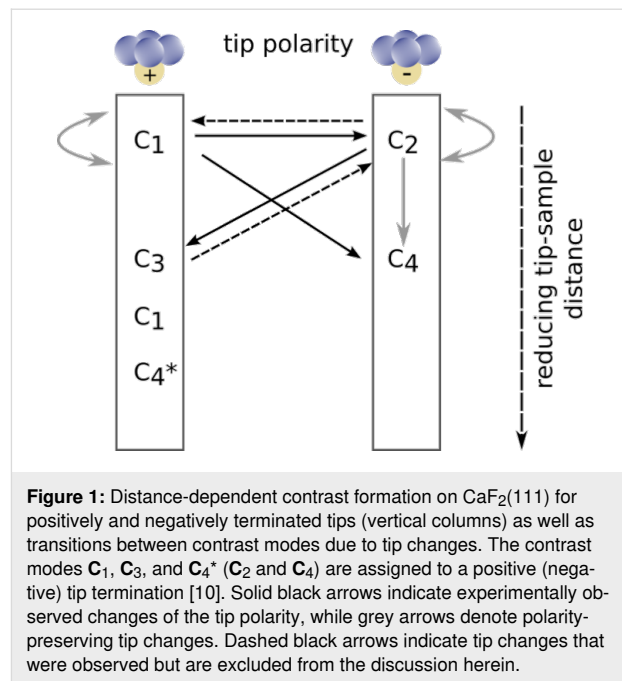


**Figure 1:** Distance-dependent contrast formation on  $\text{CaF}_2(111)$  for positively and negatively terminated tips (vertical columns) as well as transitions between contrast modes due to tip changes. The contrast modes  $\mathbf{C}_1$ ,  $\mathbf{C}_3$ , and  $\mathbf{C}_4^*$  ( $\mathbf{C}_2$  and  $\mathbf{C}_4$ ) are assigned to a positive (negative) tip termination [10]. Solid black arrows indicate experimentally observed changes of the tip polarity, while grey arrows denote polarity-preserving tip changes. Dashed black arrows indicate tip changes that were observed but are excluded from the discussion herein.

## Experimental

RT experiments were performed on a bulk  $\text{CaF}_2$  crystal after preparing a clean  $\text{CaF}_2(111)$  surface by cleaving the crystal in ultra-high vacuum (UHV) [23]. For the LT experiments, a  $\text{CaF}_2/\text{CaF}/\text{Si}(111)$  thin film sample was used. The sample was prepared *in situ* by first degassing a p-type Si (B-doped) sample (Institute of Electronic Materials Technology, Warsaw, Poland) for several hours after introduction into the vacuum. Second, the  $\text{Si}(111)-(7 \times 7)$  termination was formed by flash annealing cycles. Third,  $\text{CaF}_2$  material (99.9% purity) was deposited on the  $\text{Si}(111)-(7 \times 7)$  surface from an EFM3T e-beam sublimator (Focus GmbH, Huenstetten, Germany) at substrates temperatures of 550 °C. Under these conditions, a  $\text{CaF}$  interface layer is formed, which removes the  $\text{Si}(7 \times 7)$  reconstruction and allows for growing multilayers of well-ordered  $\text{CaF}_2(111)$  [24,25], see [26] for further preparation details.

RT experiments were performed with a UHV 750 AFM system (RHK, Troy, MI USA) operated at a base pressure of  $7.0 \times 10^{-11}$  mbar. An  $\text{Ar}^+$  ion-sputtered silicon cantilever with an eigenfrequency of around 300 kHz and a quality factor of 22000 was used. The NC-AFM was operated in the frequency-modulation mode with an oscillation amplitude of 7.4 nm, and images shown herein were acquired in the quasi constant-height mode [18]. Frequency shift values printed in the respective images correspond to the setpoint of the feedback loop. LT experiments were performed at 77 K using a LT UHV STM/AFM (ScientaOmicron, Taunusstein, Germany) operated at a base pressure of  $5 \times 10^{-10}$  mbar. NC-AFM measurements were con-

ducted with a quartz cantilever based on a tuning fork [27] and a chemically etched tungsten tip attached to the end of the active prong. The tip was further prepared *in situ* using common STM-based approaches on the bare Si surface after introducing the sensor into the vacuum system [28]. The NC-AFM microscope was operated in the frequency-modulation mode with an oscillation amplitude of 60 pm, and images were acquired in the true constant-height mode using an atom-tracking and feed-forward system for instantaneous drift compensation [29].

All frequency shift ( $\Delta f$ ) images are presented with regions of strong attractive tip–sample interaction depicted as ‘bright’ and regions of weak attractive or repulsive interaction reproduced as ‘dark’. In NC-AFM, the frequency shift  $\Delta f$  is proportional to the weighted average of the tip–sample interaction force gradient [30]. Attractive forces mostly exhibiting a positive force gradient are considered as negative and yield a negative  $\Delta f$  according to a generally accepted convention. When acquiring data in the constant height mode, we invert  $\Delta f$  images so that a steeper force gradient appears as a brighter feature corresponding to an elevation in an image of the same feature taken in the constant frequency shift (topography) mode. Arrows in the upper right corner of  $\Delta f$  images represent the fast (horizontal) and slow (vertical) scan directions.

The surface directions for the bulk crystal exposing the (111) surface can be determined by cleaving the crystal along another surface from the {111} family [31]. For CaF<sub>2</sub> thin films grown on Si(111) surfaces, it has been established that the film grows in type-B epitaxy [24,25,32]. This implies that the [112] direction of the silicon crystal surface points in opposite direction of the [112] direction of the CaF<sub>2</sub> thin film. The [112] direction of the pristine Si(111) (7 × 7) surface was determined by identi-

fying the faulted and unfaulted halves of the (7 × 7) reconstructed unit cell from STM imaging [33]. With the surface orientation established, the sublattices can be identified through a distance-dependent analysis of NC-AFM images [10], and corresponding model drawings of the CaF<sub>2</sub>(111) surface geometry are superimposed on the image data.

To improve the signal-to-noise ratio of the  $\Delta f$  data in the RT experiments, unit cell averaging is performed as described in [10]. From the unit-cell averaged data, contrast profile lines  $\Delta f_{\langle\text{uc}\rangle}$  are extracted along the diagonal of the unit cell in the [112] direction, with the resulting data included as traces next to the respective NC-AFM images.

## Results and Discussion

In Figure 2, we present RT data showing two examples of abrupt contrast changes where the polarity of the tip is maintained (polarity-preserving tip changes) but a different atomic contrast appears. The occurrences of tip changes are marked by the two chevron arrows framing the respective scan line. The nature of these changes as polarity preserving can be assessed from the contrast profiles shown in Figure 2b,c,e,f based on the conclusions in [10]. The image in Figure 2a maintains contrast mode C<sub>1</sub>, yet with an abrupt change in intensity (see Figure 2b,c), while the contrast change present in Figure 2d represents a transition from contrast mode C<sub>4</sub> (see Figure 2f) to contrast mode C<sub>2</sub> (see Figure 2e). The assignment of the contrast mode C<sub>4</sub> follows a distance-dependent analysis of the data acquired prior to this image (data not shown). Positioning the CaF<sub>2</sub>(111) surface models in Figure 2a and Figure 2d relative to the NC-AFM data is based on the sublattice analysis of the contrast profiles shown in Figure 2b,c and Figure 2e,f, respectively. This positioning indicates that there is no lateral

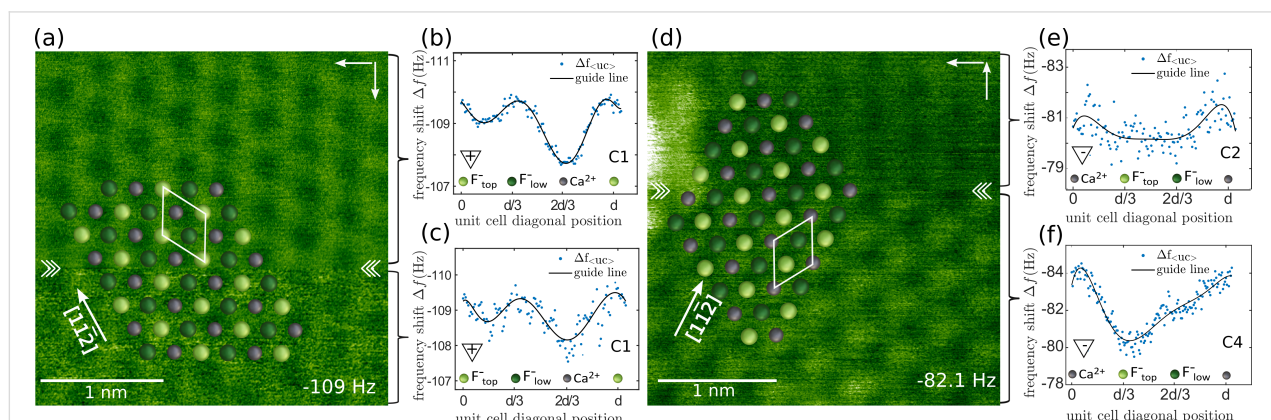


**Figure 2:** Examples of polarity-preserving tip changes on CaF<sub>2</sub>(111) at room temperature. (a, d)  $\Delta f$  data acquired at (a)  $\Delta f_{\text{set}} = -109$  Hz and (d)  $-82.1$  Hz with a top view CaF<sub>2</sub>(111) surface model overlaid. (b, c) and (e, f) Contrast profiles extracted along the [112] direction of the unit-cell averaged data from image regions indicated by the square brackets.  $d = a_0\sqrt{3}/2$  represents the distance between equivalent atoms along (11-2) directions, where  $a_0$  is the bulk lattice constant of CaF<sub>2</sub>. Atomic assignment follows the model introduced in [10], with the solid line in panels (b, c, e, f) representing a polynomial fit of degree seven as a guide to the eye.

shift involved during the tip changes as the same lattice fits well before and after the tip changes. While this is true for the NC-AFM images shown here, images indicating a lateral shift upon a tip change are commonly observed. The assignment to a polarity-preserving tip change is based on the finding that for Figure 2a, the contrast mode **C**<sub>1</sub> is related to a positively terminated tip, whereas for Figure 2d, the contrast modes **C**<sub>2</sub> and **C**<sub>4</sub> are both explained by a negatively terminated tip.

Next, we discuss tip changes that modify the tip polarity with exemplary data for negative-to-positive and positive-to-negative transitions reproduced, respectively, in Figure 3a and Figure 3d. In particular, the image data in Figure 3a recorded at RT and the corresponding contrast profiles (Figure 3b,c) exemplify a contrast change from **C**<sub>2</sub> (associated with a negatively terminated tip) to **C**<sub>3</sub> (associated with a positively terminated tip). In contrast, the image data in Figure 3d acquired at LT and the corresponding contrast profiles (Figure 3e,f) show an abrupt change from contrast mode **C**<sub>1</sub> to **C**<sub>4</sub>, implying a change from a positive to a negative tip termination. To maintain stable imaging, the tip was retracted by about 100 pm immediately after the tip change, explaining the abrupt change in image contrast. Based on the sublattice identification in the contrast profiles in Figure 3b,c and Figure 3e,f, we superimpose the CaF<sub>2</sub>(111) surface model to the data in Figure 3a and Figure 3d and furthermore find that the tip change clearly goes along with a change in polarity of the contrast forming tip cluster in both cases.

A tentative explanation for the positive-to-negative tip change is a pickup of a fluorine ion from the surface by the tip, resulting in a negative tip termination. As a consequence, the tip interacts strongly attractively with the surface Ca<sup>2+</sup> ions, explaining the contrast enhancement induced by the tip change.

During the analysis of 213 images acquired at RT, we observed 32 tip changes, with repeated evidence for polarity changes in both directions. Among these, 72% resulted in negatively terminated tips, while 28% ended in positively terminated tips. Across all 213 analyzed images, 67% exhibited contrasts associated with negatively terminated tips and 33% with positively terminated tips. This consistent trend suggests that negative tip termination is the more stable configuration when imaging fluoro-rite surfaces.

An intriguing example involving a sequence of tip changes to eventually arrive in contrast mode **C**<sub>4</sub> is shown in Figure 4. Images in Figure 4a–c and Figure 4g–i represent image data acquired while step-wise decreasing the frequency shift setpoint. Such a reduction of the tip–surface distance eventually triggers tip changes. Contrast profiles for identifying the respective contrast modes are shown in Figure 4d–f and Figure 4j–l. It is found that the tip first yields contrast **C**<sub>1</sub> (associated with a positively terminated tip) but experiences a polarity-changing tip change (Figure 4b) upon approach to the surface from contrast **C**<sub>1</sub> to **C**<sub>2</sub> (negatively terminated tip). Further approach reveals an unsteady **C**<sub>2</sub> contrast (Figure 4c) as evidenced by the difference in contrast strength of the contrast profiles in Figure 4f, whereby the **C**<sub>2</sub> contrast in the upper part (red contrast profile) is slightly weaker compared to that in the lower image half (blue contrast profile). A second polarity-preserving tip change is identified in the subsequent image in Figure 4g. Upon further decreasing the frequency shift setpoint, the **C**<sub>2</sub> contrast stabilizes in Figure 4g to Figure 4h and eventually develops to contrast **C**<sub>4</sub> (negatively terminated tip) in Figures 4i,l at further reduced tip–sample distance. While the evolution of contrast mode **C**<sub>2</sub> to **C**<sub>4</sub> is readily explained by the distance-dependence of imaging CaF<sub>2</sub>(111) with a negative tip [10], this series clearly shows the change from a previously pos-

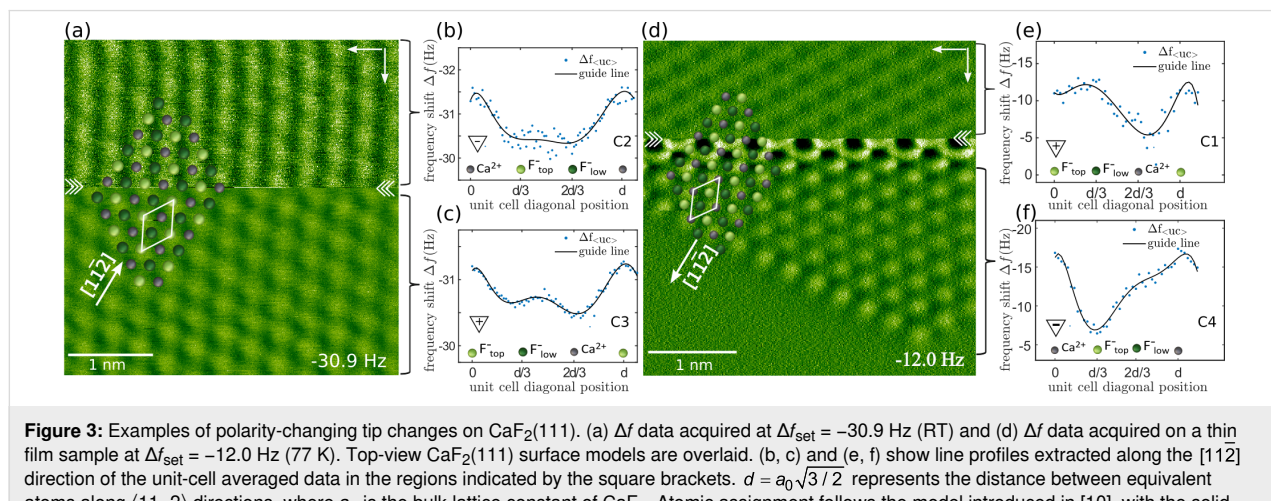


**Figure 3:** Examples of polarity-changing tip changes on CaF<sub>2</sub>(111). (a)  $\Delta f$  data acquired at  $\Delta f_{\text{set}} = -30.9$  Hz (RT) and (d)  $\Delta f$  data acquired on a thin film sample at  $\Delta f_{\text{set}} = -12.0$  Hz (77 K). Top-view CaF<sub>2</sub>(111) surface models are overlaid. (b, c) and (e, f) show line profiles extracted along the [112] direction of the unit-cell averaged data in the regions indicated by the square brackets.  $d = a_0 \sqrt{3/2}$  represents the distance between equivalent atoms along (112) directions, where  $a_0$  is the bulk lattice constant of CaF<sub>2</sub>. Atomic assignment follows the model introduced in [10], with the solid line in panels (b, c, e, f) representing a polynomial fit of degree seven as a guide to the eye.

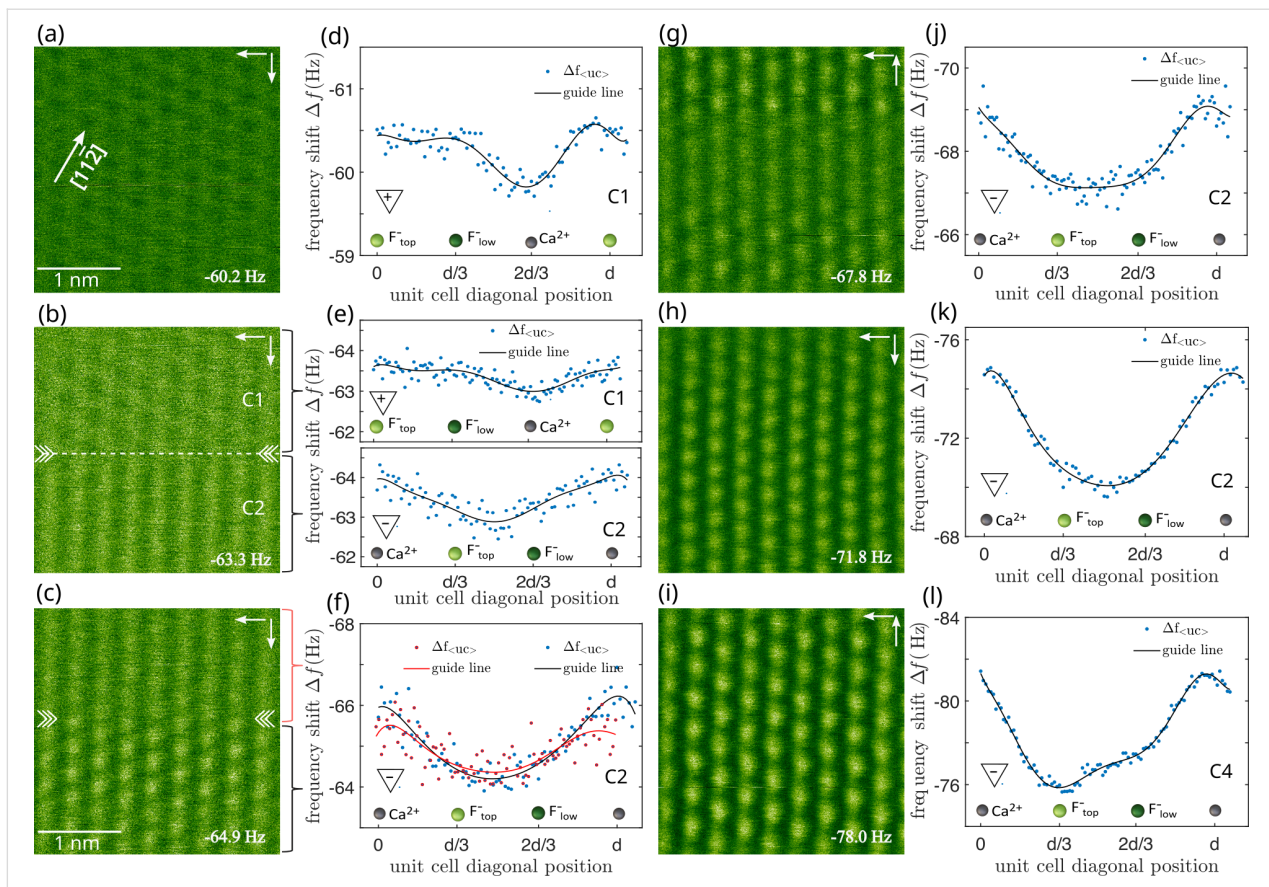


**Figure 4:** Tip changes leading to a successively stabilizing negative tip termination. (a–c) and (g–i)  $\Delta f$  data acquired while step-wise decreasing the tip–sample distance ( $\Delta f_{\text{set}} = -60.2$  Hz to  $-78.0$  Hz). (d–f) and (j–l) Line profiles extracted along the  $[1\bar{1}2]$  direction of the unit-cell averaged data.  $d = a_0\sqrt{3}/2$  represents the distance between equivalent atoms along  $(11\bar{2})$  directions, where  $a_0$  is the bulk lattice constant of  $\text{CaF}_2$ . Atomic assignment follows the model introduced in [10], with the solid line in panels (d–f) and (j–l) representing a polynomial fit of degree seven as a guide to the eye.

itively terminated tip to a negatively terminated tip finally attaining a stable configuration.

Unlike in the RT data, where we observe both polarity-preserving and polarity-changing tip changes, at low temperature, so far no polarity-preserving tip changes were observed. This is a plausible result as tip stability is generally considered a merit of LT measurements. However, conclusions drawn from LT data are based on a much smaller number of measurements than those for RT data, and we anticipate that polarity-preserving tip changes at low temperature would be found as rare events in a sample of measurements with higher statistical significance.

## Conclusion

In conclusion, we present NC-AFM data demonstrating tip changes on a bulk  $\text{CaF}_2(111)$  surface at room temperature and on a  $\text{CaF}_2/\text{CaF}/\text{Si}(111)$  thin film surface at 77 K. We demonstrate the effect of tip changes on the contrast formation and find, as a key result, routes for a discrimination between

polarity-preserving tip changes and tip changes associated with a change in tip polarity. Experimental evidence of both cases is found, with a tendency for negative tip termination to be the more stable configuration. We tentatively interpret this finding as a result of picking up a surface fluorine ion by the tip.

## Acknowledgements

P. R. gratefully acknowledges experimental support and discussions regarding the 77 K data with Philip Moriarty and Adam Sweetman.

## Funding

The authors gratefully acknowledge funding from the Deutsche Forschungsgemeinschaft (DFG) via grant RA2832/1-1 and from FP7/2007-2013 under REA grant number 628439.

## Author Contributions

Bob Kyeune: conceptualization; data curation; formal analysis; investigation; visualization; writing – original draft; writing – review & editing. Philipp Rahe: conceptualization; data cura-

tion; funding acquisition; investigation; resources; writing – review & editing. Michael Reichling: conceptualization; funding acquisition; project administration; resources; supervision; validation; writing – review & editing.

## ORCID® IDs

Bob Kyeyune - <https://orcid.org/0000-0001-9078-909X>

Philipp Rahe - <https://orcid.org/0000-0002-2768-8381>

Michael Reichling - <https://orcid.org/0000-0003-3186-9000>

## Data Availability Statement

Data generated and analyzed during this study is available from the corresponding author upon reasonable request.

## References

- Albrecht, T. R.; Grütter, P.; Horne, D.; Rugar, D. *J. Appl. Phys.* **1991**, *69*, 668–673. doi:10.1063/1.347347
- Morita, S.; Abe, M.; Yokoyama, K.; Sugawara, Y. *J. Cryst. Growth* **2000**, *210*, 408–415. doi:10.1016/s0022-0248(99)00720-4
- Morita, S.; Sugimoto, Y.; Oyabu, N.; Nishi, R.; Custance, O.; Sugawara, Y.; Abe, M. *J. Electron Microsc.* **2004**, *53*, 163–168. doi:10.1093/jmicro/53.2.163
- Schütte, J.; Rahe, P.; Tröger, L.; Rode, S.; Bechstein, R.; Reichling, M.; Kühnle, A. *Langmuir* **2010**, *26*, 8295–8300. doi:10.1021/la904706p
- Rahe, P.; Schütte, J.; Kühnle, A. *J. Phys.: Condens. Matter* **2012**, *24*, 084006. doi:10.1088/0953-8984/24/8/084006
- Liebig, A.; Hapala, P.; Weymouth, A. J.; Giessibl, F. *J. Sci. Rep.* **2020**, *10*, 14104. doi:10.1038/s41598-020-71077-9
- Pavliček, N.; Gross, L. *Nat. Rev. Chem.* **2017**, *1*, 0005. doi:10.1038/s41570-016-0005
- Foster, A. S.; Barth, C.; Shluger, A. L.; Reichling, M. *Phys. Rev. Lett.* **2001**, *86*, 2373–2376. doi:10.1103/physrevlett.86.2373
- Hoffmann, R.; Weiner, D.; Schirmeisen, A.; Foster, A. S. *Phys. Rev. B* **2009**, *80*, 115426. doi:10.1103/physrevb.80.115426
- Kyeyune, B.; Olbrich, R.; Reichling, M.; Rahe, P. *Phys. Rev. B* **2024**, *110*, 155417. doi:10.1103/physrevb.110.155417
- Liebig, A.; Peronio, A.; Meuer, D.; Weymouth, A. J.; Giessibl, F. *J. New J. Phys.* **2020**, *22*, 063040. doi:10.1088/1367-2630/ab8efd
- Jiménez-Sánchez, M. D.; Nicoara, N.; Gómez-Rodríguez, J. M. *Appl. Surf. Sci.* **2021**, *542*, 148669. doi:10.1016/j.apsusc.2020.148669
- Kawai, S.; Foster, A. S.; Björkman, T.; Nowakowska, S.; Björk, J.; Canova, F. F.; Gade, L. H.; Jung, T. A.; Meyer, E. *Nat. Commun.* **2016**, *7*, 11559. doi:10.1038/ncomms11559
- Mohn, F.; Schuler, B.; Gross, L.; Meyer, G. *Appl. Phys. Lett.* **2013**, *102*, 073109. doi:10.1063/1.4793200
- Bamidele, J.; Kinoshita, Y.; Turanský, R.; Lee, S. H.; Naitoh, Y.; Li, Y. J.; Sugawara, Y.; Štich, I.; Kantorovich, L. *Phys. Rev. B* **2012**, *86*, 155422. doi:10.1103/physrevb.86.155422
- Mönig, H.; Amirjalayer, S.; Timmer, A.; Hu, Z.; Liu, L.; Díaz Arado, O.; Cnudde, M.; Strassert, C. A.; Ji, W.; Rohlfing, M.; Fuchs, H. *Nat. Nanotechnol.* **2018**, *13*, 371–375. doi:10.1038/s41565-018-0104-4
- Wiesener, P.; Förster, S.; Merkel, M.; Schulze Lammers, B.; Fuchs, H.; Amirjalayer, S.; Mönig, H. *ACS Nano* **2024**, *18*, 21948–21956. doi:10.1021/acsnano.4c03155
- Barth, C.; Foster, A. S.; Reichling, M.; Shluger, A. L. *J. Phys.: Condens. Matter* **2001**, *13*, 2061–2079. doi:10.1088/0953-8984/13/10/303
- Hoffmann, R.; Kantorovich, L. N.; Baratoff, A.; Hug, H. J.; Güntherodt, H.-J. *Phys. Rev. Lett.* **2004**, *92*, 146103. doi:10.1103/physrevlett.92.146103
- Foster, A. S.; Shluger, A. L.; Nieminen, R. M. *Nanotechnology* **2004**, *15*, S60–S64. doi:10.1088/0957-4484/15/2/013
- Pou, P.; Ghasemi, S. A.; Jelinek, P.; Lenosky, T.; Goedecker, S.; Pérez, R. *Nanotechnology* **2009**, *20*, 264015. doi:10.1088/0957-4484/20/26/264015
- Yurtsever, A.; Fernández-Torre, D.; González, C.; Jelínek, P.; Pou, P.; Sugimoto, Y.; Abe, M.; Pérez, R.; Morita, S. *Phys. Rev. B* **2012**, *85*, 125416. doi:10.1103/physrevb.85.125416
- Tröger, L.; Schütte, J.; Ostendorf, F.; Kühnle, A.; Reichling, M. *Rev. Sci. Instrum.* **2009**, *80*, 063703. doi:10.1063/1.3152367
- Olmstead, M. A. Heteroepitaxy of Disparate Materials: From Chemisorption to Epitaxy in  $\text{CaF}_2/\text{Si}(111)$ . In *Thin Films: Heteroepitaxial Systems*; Liu, W. K.; Santos, M. B., Eds.; Series on Directions in Condensed Matter Physics; World Scientific: Singapore, 1999; pp 211–266. doi:10.1142/9789812816511\_0005
- Wollschläger, J. Resonant tunneling devices based on epitaxial insulator-semiconductor structures: growth and characterisation of  $\text{CaF}_2$  films on  $\text{Si}(111)$ . In *Recent Research Developments in Applied Physics*; Pandalai, S. G., Ed.; Transworld Research Network: Trivandrum, India, 2002; Vol. 5-II, pp 621–695.
- Rahe, P.; Smith, E. F.; Wollschläger, J.; Moriarty, P. *J. Phys. Rev. B* **2018**, *97*, 125418. doi:10.1103/physrevb.97.125418
- Giessibl, F. *J. Appl. Phys. Lett.* **1998**, *73*, 3956–3958. doi:10.1063/1.122948
- Sweetman, A.; Stirling, J.; Jarvis, S. P.; Rahe, P.; Moriarty, P. *Phys. Rev. B* **2016**, *94*, 115440. doi:10.1103/physrevb.94.115440
- Rahe, P.; Schütte, J.; Schniederberend, W.; Reichling, M.; Abe, M.; Sugimoto, Y.; Kühnle, A. *Rev. Sci. Instrum.* **2011**, *82*, 063704. doi:10.1063/1.3600453
- Söngen, H.; Bechstein, R.; Kühnle, A. *J. Phys.: Condens. Matter* **2017**, *29*, 274001. doi:10.1088/1361-648x/aa6f8b
- Kyeyune, B.; Olbrich, R.; Rahe, P.; Reichling, M. *Rev. Sci. Instrum.* **2024**, *95*, 023702. doi:10.1063/5.0182520
- Wollschläger, J. *Appl. Phys. A: Mater. Sci. Process.* **2002**, *75*, 155–166. doi:10.1007/s003390101064
- Sugimoto, Y.; Yi, I.; Morita, K.-i.; Abe, M.; Morita, S. *Appl. Phys. Lett.* **2010**, *96*, 263114. doi:10.1063/1.3457997

## License and Terms

This is an open access article licensed under the terms of the Beilstein-Institut Open Access License Agreement (<https://www.beilstein-journals.org/bjnano/terms>), which is identical to the Creative Commons Attribution 4.0 International License (<https://creativecommons.org/licenses/by/4.0>). The reuse of material under this license requires that the author(s), source and license are credited. Third-party material in this article could be subject to other licenses (typically indicated in the credit line), and in this case, users are required to obtain permission from the license holder to reuse the material.

The definitive version of this article is the electronic one which can be found at:

<https://doi.org/10.3762/bjnano.16.72>